Conformation-induced separation of 3-Chloropropene from 1-Chloropropane through nanoporous monolayer graphenes

Journal:	*Physical Chemistry Chemical Physics*
Manuscript ID	CP-COM-01-2019-000137.R1
Article Type:	Paper
Date Submitted by the Author:	29-Jan-2019
Complete List of Authors:	Xu, Yinxiang; Sichuan University of Science & Engineering, College of Mechanical Engineering; Sichuan University of Science & Engineering, College of Mechanical Engineering Zhang, Yujia; Chinese Academy of Sciences, Wang, Steven; Newcastle University, School of Chemical Engineering and Advanced Materials Xu, Junbo; Institute of Process Engineering, Chinese Academy of Sciences, Key Laboratory of Green Process and Engineering Yang, Chao; Institute of Process Engineering, Chinese Academy of Sciences, CAS Key Laboratory of Green Process and Engineering

Conformation-induced separation of 3-Chloropropene from 1-Chloropropane through nanoporous monolayer graphenes

Yinxiang Xu[a,b,c], Yujia Zhang [c,d], Steven Wang[e], Junbo Xu[c,*] and Chao Yang[c,d,*]

[a] School of Space and Environment, Beihang University, Beijing 100191, China

[b] College of Mechanical Engineering, Sichuan University of Science and Engineering, Sichuan 643000, China

[c] CAS Key Laboratory of Green Process and Engineering, Institute of Process Engineering, Chinese Academy of Sciences, Beijing 100190, China

[d] University of Chinese Academy of Sciences, Beijing 100190, China

[e] School of Engineering, Newcastle University, NE1 7RU, UK

Abstract

Achieving ultrahigh selectivity for separating paraffin/olefin mixtures with physical and chemical similarity, especially for halohydrocarbon, is a long-standing challenge in high-purity polymer production. We explored three H-saturated nanoporous graphene (NG) membranes with appropriate pore geometries that can achieve the complete exclusion of 1-Chloropropane (C_3H_7Cl) from C_3H_5Cl during the molecular dynamics simulations. Inferred from thermodynamics calculations, C_3H_5Cl has the lower energy barrier of penetration than C_3H_7Cl and the NG membranes show preferential adsorption to C_3H_5Cl, which facilitate the penetration of C_3H_5Cl through the pores. The conformational energy analysis of the two molecules shows that C_3H_5Cl has the lower energy penalty to twist to the molecular conformation that nanopores preferred than C_3H_7Cl, which mainly determines the ultrahigh selectivity for C_3H_5Cl. We anticipate that the conformation-induced mechanism outlined here can provide a reference to separate paraffin/olefin mixtures with the distinct difference of conformational energy profiles.

* Corresponding authors: jbxu@ipe.ac.cn (J.B. Xu); chaoyang@ipe.ac.cn (C. Yang)

Keywords: nanoporous graphene membrane, conformation-induced mechanism, energy barrier, paraffin/olefin separation

1. Introduction

Highly selective separation of low-carbon paraffin/olefin mixtures with physicochemical similarity is of great importance and difficulty in the high-purity polymer production where the impurity with a low content (≤1%) may continuously accumulate in the reaction system to influence the production process[1-3]. Especially, it is a greater challenge to separate the halohydrocarbon mixtures due to that the halogenated groups may shorten the difference between olefins and paraffins. As a special case, under the influence of the chlorine group, the separation of 1-Chloropropane (C_3H_7Cl) and 3-Chloropropene (C_3H_5Cl), where C_3H_5Cl is an essential intermediate in the epoxy resin and glycerol production, is far more difficult than that of C_3H_6/C_3H_8 owing to their closer properties, especially for the polarity (Table S1). Commercially, the separation of light hydrocarbons is mainly accomplished by means of cryogenic distillation in a column containing over 100 trays[4]. Undoubtedly, the process is highly energy-intensive. As an alternatively energy-efficient approach, membrane-based technology has the promising potential to separate paraffin/olefin mixtures by distinguishing the differences in molecular sizes[5], shapes[6] and polarities[7]. Some closely related molecules (e.g., C_3H_8/C_3H_6) have been successfully separated by screening appropriate pore structures from dozens of silica[8], zeolites[9], metal organic frameworks[10], carbon[11] and other materials[12-14]. However, the screening is still time-consuming.

Recently, nanoporous graphene (NG) with one-atom thickness has been demonstrated as an ideal separation membrane[15]. The nanopores with specific shapes and sizes can be formed by removing carbon atoms in a pristine monolayer grapheme, which may be experimentally realized

through ion bombardment[16, 17], electron beam treatment[18], or oxidative etching[19]. Both experimental and theoretical studies have indicated that such NG membranes exhibited ultrahigh selectivity and excellent permeability in the separation of similar mixtures[20-22]. For example, Liu et al.[23] reported that the nitrogen-functionalized NG membrane showed a CO_2 permeance of 2.9×10^5 GPU (gas permeance unit, 1 GPU=3.35×10^{-10} mol·s^{-1}·m^2·Pa^{-1}) and the selectivity of CO_2/N_2 was around 300. Li et al.[13] experimentally demonstrated that the NG membranes exhibited a high selectivity of 3400 for H_2/CO_2 and 900 for H_2/N_2. However, most works were focused on natural gases with simple structures (e.g., $H_2/H_2S/CO_2/N_2$[24, 25]) and a few reports are involved in C_3-C_4 hydrocarbons (e.g., C_3H_8/C_3H_6[26]). To our best knowledge, no literature has reported the separation of mixed halohydrocarbons with ultrahigh selectivity, and explorative studies indicated that available separation mechanisms such as the π complexation–driven method[27] were inefficient to separate C_3H_5Cl/C_3H_7Cl mixtures into individual compounds. Thus, the usable pore geometries and separation mechanism should be developed.

In this paper, we focus on constructing appropriate pores with molecular recognition ability to C_3H_5Cl in a pristine monolayer graphene and revealing the separation mechanisms by molecular dynamics (MD) simulations and density functional theory (DFT) calculations. We also investigate the effect of the degree of membrane flexibility on the pore geometries and separation performance by gradually relaxing 1~4 carbon layers outward from the pore center. We anticipate the work can provide the theoretical guidance in the effective separation of halogenated paraffin/olefin mixtures through NG membranes. The obtained pore geometries can also provide a reference for the pore screening in the existing porous materials (e.g., zeolite and silica).

2. Models and methods

2.1 Molecular dynamics simulations

We performed non-equilibrium molecular dynamics (NEMD) simulations to investigate the separation performance of C_3H_7Cl and C_3H_5Cl through the NG membranes in a non-equilibrium system. As shown in Figure 1, the NG membrane of 29.82 Å × 29.52 Å divided the simulation box of width 138.64 Å into two chambers, the left of which was filled with an equal number of 100 molecules of C_3H_5Cl and C_3H_7Cl. The other chamber was a vacuum region of width 93.1 Å. In the NEMD simulations, the molecules were driven by pressure difference between the two chambers. The simulations were performed on basis of the consistent-valence force field (CVFF) implemented in LAMMPS (Large-scale Atomic/Molecular Massively Parallel Simulator) packages[28, 29]. The Lorenta-Berthelot mixing rules were used to determine all of the Lennard-Jones cross potential parameters between molecule/graphene and graphene/graphene interactions. The Lennard-Jones parameters are listed in Table 1. Periodic boundary conditions were applied in *xyz* directions and an impermeable He wall was placed in the end of the left chamber to prevent molecules from crossing the *z*-direction periodic boundary. The simulation was performed using a NVT-ensemble at 350 K with a Nose-Hoover thermostat for temperature control. The fixed timestep was 1 fs. The cutoff for Lennard-Jones and Coulombic interactions was 10 Å, and the Ewald method was used to calculate the long-range electrostatic interactions.

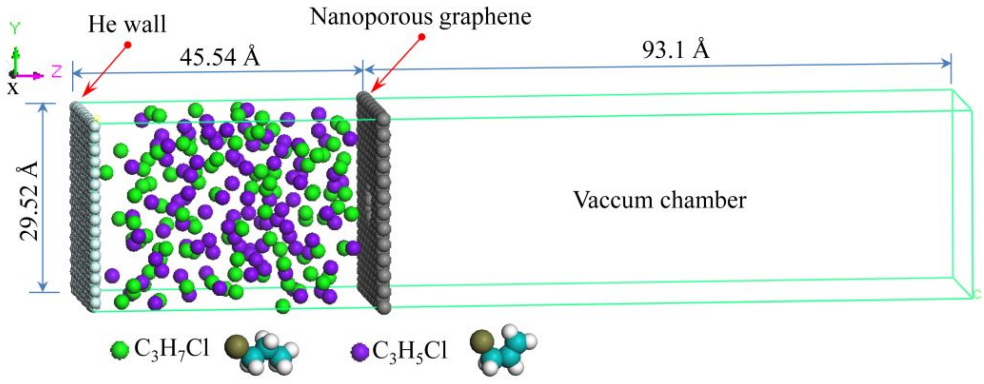

Figure 1. Simulation box with 100 C_3H_7Cl and 100 C_3H_5Cl molecules into the left chamber.

Table 1. Lennard-Jones parameters used in molecular dynamics simulation

	ε/k_B (K)	σ (Å)
C (sp^2)	74.48	3.62
C (sp^3)	19.63	3.88
H	19.12	2.45
Cl	34.76	3.54

2.2 Pore design

To find highly selective NG membranes for C_3H_7Cl/C_3H_5Cl separation, we constructed twelve pores with different geometrical shapes (e.g., Oval) and sizes by removing 13~24 carbon atoms on a perfect graphene sheet (Figure 2). All the dangling bonds were saturated with the positively charged hydrogen atoms and the nanopores were named according to the number of drilled atoms. The H-pore-16 membrane has been investigated to separate the similar N_2/CO_2 mixture[30, 31]. Before simulations, the structures of all the membranes have been optimized by DFT calculations, as detailed in the next section.

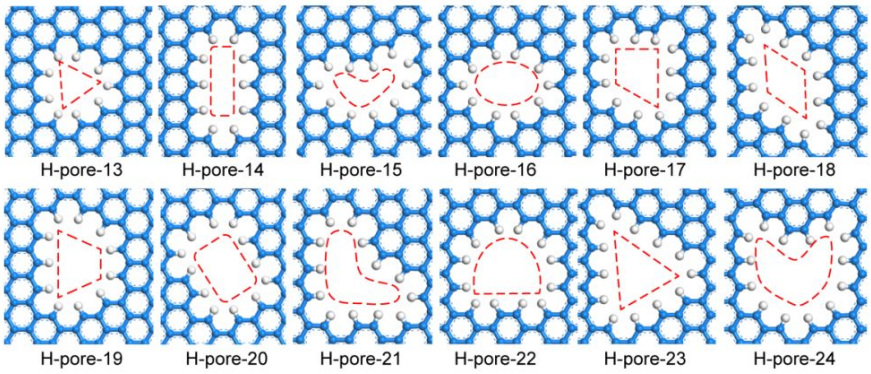

Figure 2. Pore models with different geometrical shapes and sizes by removing 13~24 carbon atoms on a pristine graphene sheet

To our knowledge, the experimental realization of the ideal NG membranes remains challenging. However, there are two promising approaches based on extensive experimental efforts[32], including the "top-down" fabrication by creating pores in a pristine material and the "bottom-up" synthesis of a porous material. In the "top-down" approach, the ion irradiation combining with edge-selective electron recoil sputtering can be used to create atomic-scale pores with radii as small as 3 Å[33] and then the dangling bonds can be saturated by hydrogen. Another approach is to directly synthesize the basic building blocks constituting the structures in Figure 2 and then assemble them by the covalently cross-linking method. This technology has been successfully applied to synthesize a two-dimensional polymer with an ultrahigh density of ~7 Å nanopores[34]. It follows that these successes provide the potential pathway to synthesize uniform and appropriately sized nanopores in our study.

2.3 Density functional theory calculation

DFT calculations were performed with the generalized gradient approximation (GGA) of the Perdew-Burke-Emzerhof (PBE) form in the Dmol3 module[35, 36]. The Tkatchenko-Scheffler method for DFD-D correction[37] was applied. The electron core was treated by effective core potentials (ECP). The double numerical atomic orbital augmented by d-polarization function (DNP) was used as the basis set. The tolerance of self-consistent field (SCF) was 10^{-6} au. The convergence criterion for DFT calculations was 1×10^{-5} Ha for total energy, 2×10^{-3} Ha/Å for force, and 5×10^{-3} Ha for displacement. The global cutoff radius was 3.8 Å. The DFT method was used to fully optimize the structure of porous graphene. The vacuum spacing of 40 Å was applied in the *z* direction to avoid interactions between periodic images. The Hirshfeld charges and ESP charges, calculated by DFT, were employed to the nanoporous graphene (NG) membrane and C_3H_5Cl/C_3H_7Cl molecules, respectively (Figure S1-S2).

3. Results and discussion

3.1 Separation performance of C_3H_7Cl/C_3H_5Cl through different NG membranes

NEMD simulations were performed to investigate the separation performance of C_3H_7Cl/C_3H_7Cl mixtures through twelve NG models with different geometries and sizes. Considering that freezing the pore may lead to unrealistic C-C-H bond angles due to that the suspended C-H bonds have a large flexibility[38], the H atoms and the first carbon layer around the pore were flexible to allow possible deformations of the edge of the nanopores during the NEMD simulations. As shown in Figure 3 and S5, during the 100-ns NEMD simulations, no C_3H_7Cl was observed to penetrate through H-pore-16, H-pore-18 and H-pore-21, thereby exhibiting the ultrahigh selectivity for C_3H_5Cl. However, other membranes have the low selectivity (Table 2). This is because that the smaller sizes of H-pore-11, H-pore-12 and H-pore-13 restrain the transport of C_3H_5Cl and C_3H_7Cl molecules, while H-pore-22, H-pore-23 and H-pore-24 are overlarge to allow the both molecules to cross. Additionally, the pore shapes also influence the permselectivity. Even if only one carbon atom was added or subtracted, the selectivity of the pores changed significantly. For example, H-pore-17 with a good likeness of right trapezoid exhibits low selectivity for C_3H_5Cl after removing one atom from H-pore-16 with an excellent likeness of oval. This reveals that the special shape of H-pore-16 is more suitable for flexible C_3H_5Cl permeation with specific molecular orientations than that of H-pore-17, and so are H-pore-18 and H-pore-21. Therefore, we successfully explored three basic pore geometries to separate C_3H_5Cl/C_3H_7Cl with a size difference of ~0.2 Å (Figure S3). To assess the stability and reliability of the results, we expanded the molecular chamber to be 2×2×2 supercells with 800 C_3H_5Cl and 800 C_3H_7Cl for a 28-ns MD simulation, and the results demonstrate that no C_3H_7Cl can cross H-pore-16, H-pore-18 and H-pore-21 membranes (Figure S6). In addition, the chosen membranes maintain a perfect permselectivity within a large range of initial densities in the molecular chamber (Figure S7).

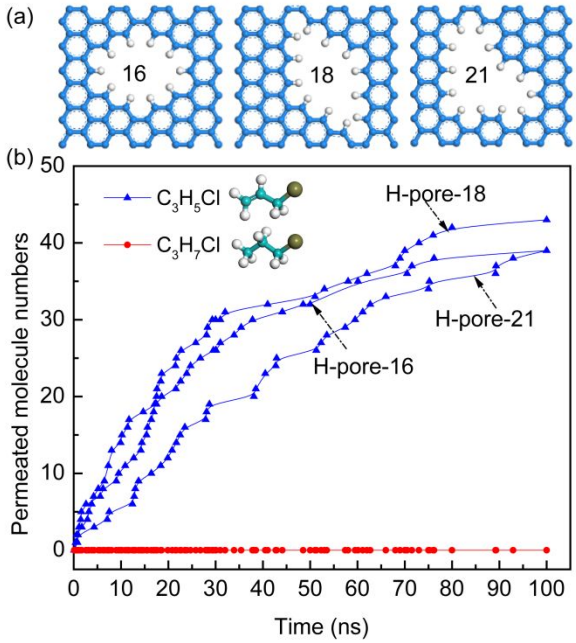

Figure 3. (a) H-saturated nanoporous graphenes: H-pore-16 (left), H-pore-18 (middle) and H-pore-21 (right); (b) the number profiles of penetrated molecules for C_3H_5Cl and C_3H_7Cl (1:1) passing through the pores at 350 K.

Table 2. Number of permeated C_3H_7Cl and C_3H_5Cl molecules through different pores after a 8-ns NEMD simulation

H-pores	13[a]	14	15	16	17	18	19	20	21	22	23	24
C_3H_5Cl	0	0	0	13	36	9	44	41	5	54	55	46
C_3H_7Cl	0	0	0	0	4	0	8	8	0	36	16	38

[a] Number of C atoms removed from a pristine graphene sheet

3.2 Separation mechanisms

To further rationalize the phenomena observed above, the interaction energy profiles corresponding to the molecule crossing the H-pore-16, H-pore-18 and H-pore-21 membranes were calculated through LAMMPS. Ahead of computation, it is clear that the flexible C_3H_5Cl and C_3H_7Cl

molecules appear various conformations during the penetration process, which may influence the interaction energy between the NG membranes and the molecules. We performed MD simulations to fast screen the representative membrane-molecule configurations with minimum potential energy in a given adsorption height while constraining the *z*-coordinate of the middle C atom (marked in Figure S8) in a hydrocarbon molecule. The molecule can freely rotate, twist and translate in *x* and *y* directions. The system was equilibrated at different adsorption heights for 2 ns with a timestep of 1 fs. During the next 3-ns MD simulation, data were collected after energy minimization using a conjugate gradient algorithm with an energy delta tolerance of 10^{-4} kcal/mol every 500 ps. Subsequently, the minimum potential energy at a given adsorption height can be calculated by averaging the collected energy values. Then, we obtained the potential energy at a series of adsorption heights *z* (-15 Å to 15 Å, 42 points) along the crossing trajectory. Considering that the potential energy at *z*=15 Å can be regarded as the total energy of the isolated hydrocarbon molecule and graphene membrane, the interaction energy (E_{int}) can be defined as

$$E_{int}=E_z-E_{15} \quad (1)$$

where E_z and E_{15} are the potential energy of molecule/graphene complex when the hydrocarbon molecule is located at the analyzed height *z* and *z* = 15, respectively. In this way, different parts of the interaction energy, such as van der Waals (vdW) interaction, electrostatic interaction and molecular energy (bond energy, angle energy and dihedral energy), were also recorded and presented. Different from the artificially designed path for molecules crossing the pore[39], the model in our work can rapidly obtain the critical interaction energy with stable membrane-molecule configurations at different adsorption heights.

In most cases, adsorption and penetration processes are the two important steps for hydrocarbon molecules passing through the pores. Figure 4 shows the interaction energy profiles for a single C_3H_5Cl or C_3H_7Cl penetrating the three pores as a function of the distance from the middle C of the

hydrocarbon molecule to the NG membrane (adsorption height *z*). There was a shallow potential well at the distance of 3.5 Å. The attractive well for C_3H_5Cl was deeper than that of C_3H_7Cl, which means it was easier for C_3H_5Cl to approach the pore rim of the membrane. The results are consistent with the distributions of molecular number densities along *z* axis obtained from the NEMD results (Figure 5 and S9). They shows that C_3H_5Cl and C_3H_7Cl preferred to stay at the adsorption height of 2.4~6.5 Å (denoted as adsorption layer). The number of C_3H_5Cl molecules in the adsorption layer was more than that of C_3H_7Cl, which means all the three NG membranes show stronger adsorption selectivity for C_3H_5Cl (Table S3). It was also found that the energy barrier for C_3H_7Cl passing through the pore was much higher than that for C_3H_5Cl. Roughly estimated by the energy barrier difference[40], the selectivity of the H-pore-16 membrane for C_3H_5Cl/C_3H_7Cl reached up to 1700, which means it is difficult for C_3H_7Cl to cross the pore. Even if the initial density in the molecule chamber increased to a higher value to provide an extremely high driving force, the NG membranes still had an ultrahigh selectivity for C_3H_5Cl (Figure S7). Thus, whether the molecules can easily pass through the NG membrane is determined by the energy barrier for hydrocarbon molecules getting into the pores.

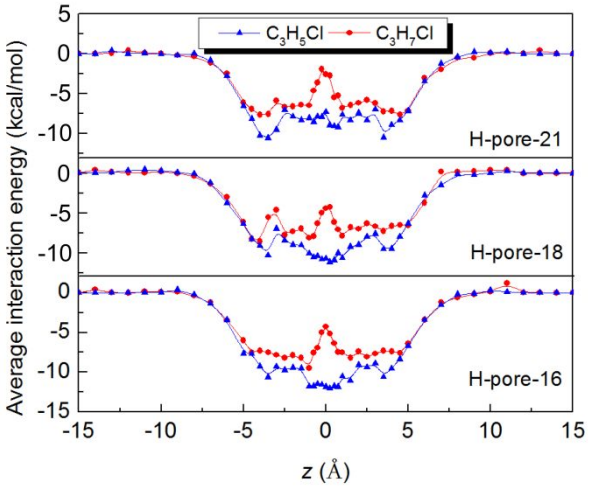

Figure 4. Interaction energy for C_3H_7Cl and C_3H_5Cl passing through the pores of H-pore-16, H-pore-18 and H-pore-21 as a function of z-coordinate of the middle C in a hydrocarbon molecule.

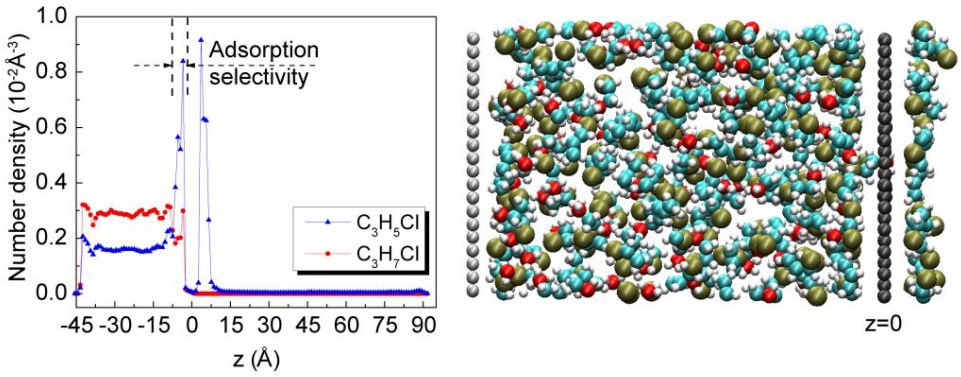

Figure 5. Average number density profiles of C_3H_5Cl and C_3H_7Cl (marked with the red C) passing through the H-pore-16 membrane along *z* axis for 1 ns and the corresponding snapshot.

To get deeper insight into the transport mechanism, we analyzed the contributions of van der Waals (vdW) forces, electrostatic interaction and molecular energy (bond energy, angle energy and dihedral energy) for interaction energy between the NG and hydrocarbon molecules along *z* axis (Figure 6). It can be found that the vdW interaction energy was largely negative, inducing strong attractive forces for hydrocarbon molecules close to the membrane surface (Figure 6a). C_3H_5Cl had a higher attractive interaction than C_3H_7Cl, which mainly contributed to the higher adsorption selectivity of C_3H_5Cl. The electrostatic interaction energy showed slight difference for C_3H_5Cl and C_3H_7Cl, and C_3H_7Cl had the higher repulsive interaction with the three NG membranes than C_3H_5Cl when located in the hole center, due to the stronger repulsive force between the passivated H and the H atoms of C_3H_7Cl (Figure 6b). We also found that no C_3H_7Cl can pass through the NG membranes with the charges of all atoms changed to zero (Figure S10), thus the molecular selectivity was independent of electrostatic interaction. On the other hand, there was a higher repulsive dihedral energy barrier for C_3H_7Cl to penetrate the pores than that for C_3H_5Cl (Figure 6d), which demonstrates that the conformation of hydrocarbon molecules affected the penetration selectivity.

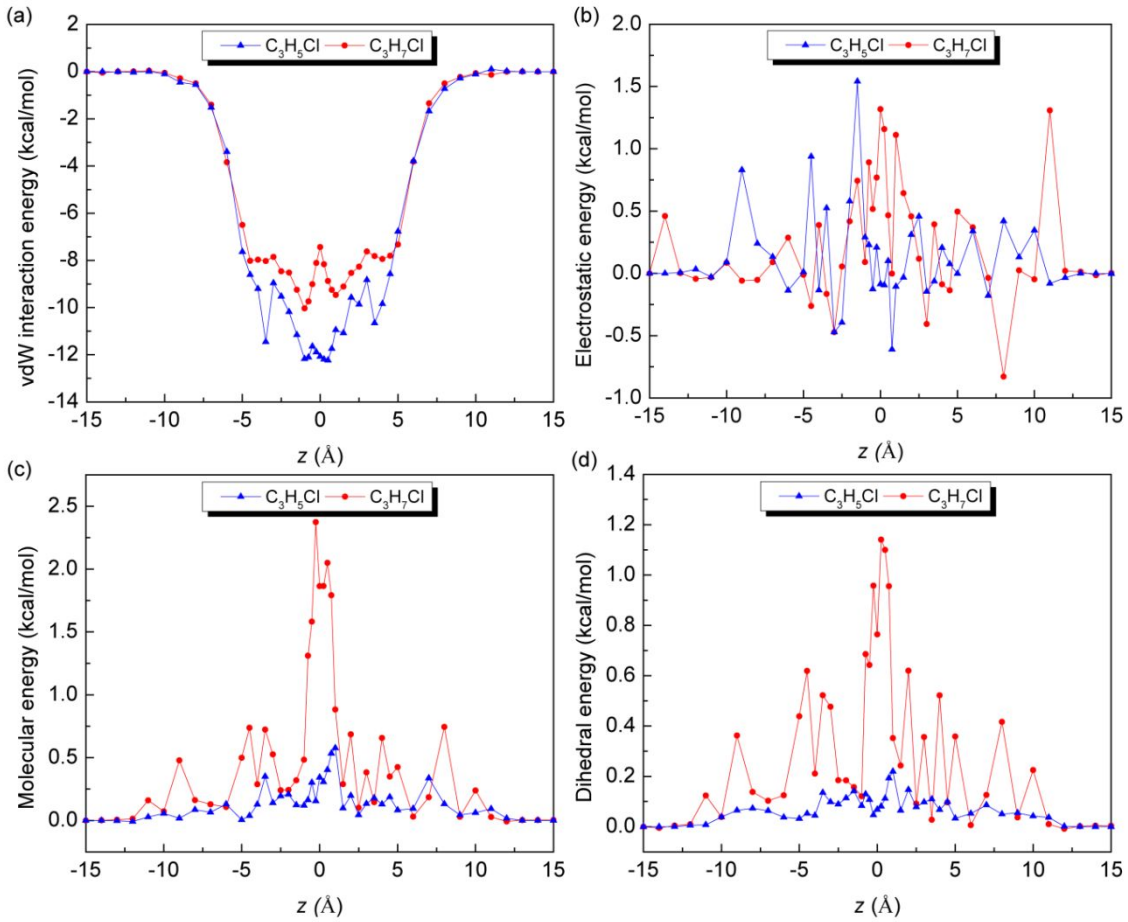

Figure 6. Distributions of (a) vdW interaction, (b) electrostatic interaction, (c) molecular energy and (d) dihedral energy as the components of the interaction energy between the H-pore-16 and hydrocarbon molecules along *z* axis.

To further explore the penetration mechanism, we captured the conformation snapshots of molecules penetrating the pores during the NEMD simulation and investigated the potential energy of C_3H_5Cl and C_3H_7Cl as a function of Cl-C-C-C dihedral angles by DFT calculations. Figure 7a displays C_3H_5Cl went across the pore by the way of twisting around the cis-conformation with a Cl-C-C-C dihedral angle of 0°. Actually, it can be frequently observed that C_3H_5Cl fluctuated around the cis-conformation during the period from the first atom entering into the pore to the last atom leaving the pore. In the whole penetration process, flexible C_3H_5Cl molecules were constantly self-regulated to match with the pore shape, size and energy fields. From the NEMD results above,

C_3H_7Cl cannot readily pass through the pore even if it has similar dimension and shape with C_3H_5Cl. To capture the penetration snapshots of C_3H_7Cl molecules, we enforced them to hurdle across the pore by pushing the He wall towards the NG membrane for an appropriate and ultrahigh pressure difference between the molecule and vacuum chambers. As shown in Figure 7b, cis-C_3H_7Cl was also able to swing into the H-pore-16 around the dihedral angle of 0°. It can be concluded that the pores in the H-pore-16, H-pore-18 and H-pore-21 prefer cis-conformation molecules (Figure S11-12). Therefore, the penetration mechanism may be related to the conformational energy difference between C_3H_5Cl and C_3H_7Cl when the flexible molecules freely rotated along their C-C single bond. As shown in Figure 7c, cis-C_3H_5Cl is the stable conformation with the lowest potential energy, while cis-C_3H_7Cl reaches its high-energy peak because of the repulsive interaction of the Cl group and methyl. It needs a large energy penalty to twist along the C-C single bond from any other angles to zero (8.26 kcal/mol). Thus, it is not easy for C_3H_7Cl to cross the three pores with the preferable access to cis-conformations. The above analyses indicates that suitable pore sizes and shapes have a strong role in controlling the molecule conformation, thus resulting in tailoring the flexibility to lower the penetrated energy penalty for obtaining high penetration selectivity of C_3H_5Cl.

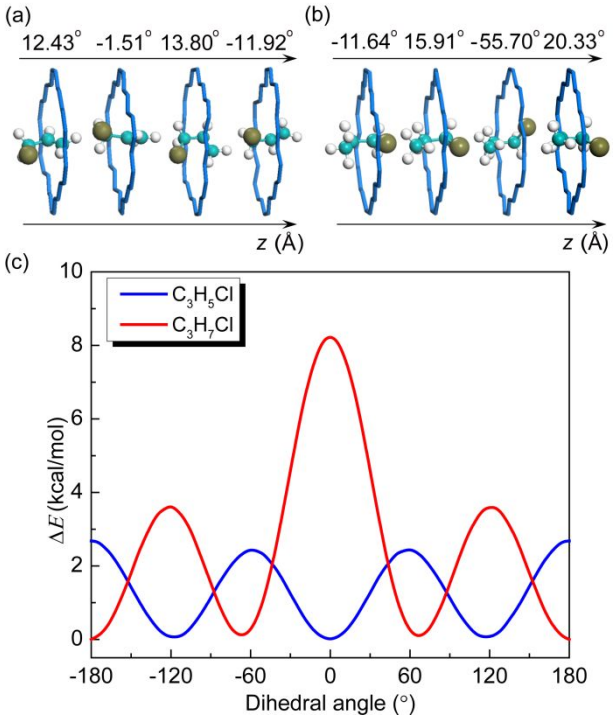

Figure 7. (a) Conformation snapshots of C_3H_5Cl passing through the H-pore-16 membrane obtained from the above NEMD simulation; (b) snapshots of C_3H_7Cl enforced to cross the H-pore-16 membrane by pushing the He wall; (c) potential energy for C_3H_5Cl and C_3H_7Cl as a function of Cl-C-C-C dihedral angles.

3.3 Effects of NG membrane flexibility

In the abovementioned cases, we only allow the rearrangement of H atoms and the first carbon layer around the pores. According to the reported literature[41], the membrane flexibility can influence the permselectivity. Here, we gradually relaxed the second, third and then fourth carbon layer near the pore to be a flexible honeycomb net for the NEMD simulations (Figures 8 and S13). For convenience, the cases with the relaxation of 1, 2, 3 and 4 carbon layers outward from the pore are named as Case-1, Case-2, Case-3 and Case-4, respectively. The number profiles of permeated C_3H_5Cl/C_3H_7Cl molecules through H-pore-16, H-pore-18 and H-pore-21 over time are shown in Figures 9 and S14. Due to the micro-deformation of pore geometries affected by membrane flexibility, a small number of C_3H_7Cl molecules were detected during the 30-ns simulations. However, the chosen membranes with an excellent flexibility still exhibit higher selectivity for C_3H_5Cl over C_3H_7Cl.

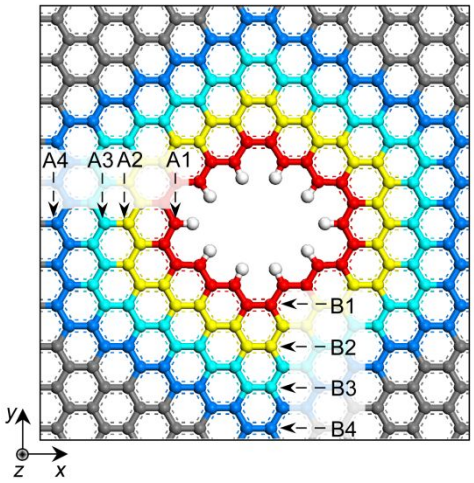

Figure 8. Honeycomb model of the flexible H atoms and 1~4 layers of C atoms around the pore in the H-pore-16 membrane during the NEMD simulation. Inserts represent the carbon atoms in different flexible layers along *x* and *y* directions.

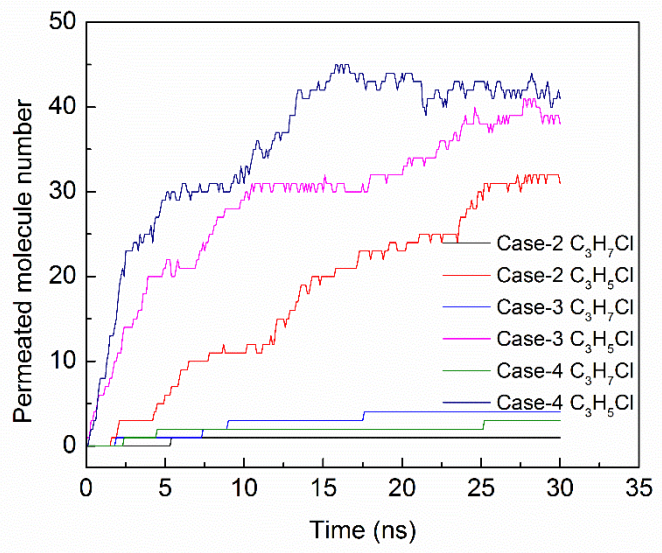

Figure 9. Number of C_3H_5Cl/C_3H_7Cl molecules permeating the H-pore-16 membrane with 1~4 carbon layers around the pore relaxed during 30-ns NEMD simulations.

For a further understanding of structure relaxation effects, we also quantified the displacements of the carbon atoms around the pore in comparison with the initial positions. According to the 3000 data points recorded along the trajectory in every case (Figure S15), we obtained the frequency distributions of the displacements (Δx, Δy and Δz) of the carbon atoms (e.g., A1~A4 and B1~B4) around the pores in the chosen three membranes within a certain range during the 30-ns NEMD simulations (Figures 10 and S16-18). As shown in Figure 10, it can be found that the distributions are the classic bell curves which frequently appear in normal distributions in statistics. In Figure 10a, the mean value μ of Δz is 0 Å in all the cases and the standard deviation σ of Δz (0.11 Å) in Case-1 is close to that (0.13 Å) in Case-4 with a higher flexibility, which demonstrates that the degree of flexibility has a little influence on the rearrangement of the carbon atoms at the pore edge in the

H-pore-16 membrane along the z direction. It can be also found that a probability of 95.44% falls within the deformation range of about -0.36 Å ~0.36 Å, which is far smaller than the C-C bond length (1.34 Å). As for Δx (Figure 10b), the distribution curves shift leftwards with the increase of structure flexibility which enhances the C-C bond stretch. The mean values μ of Δx are -0.08 Å in Case-1, -0.12 Å in Case-2, -0.14 Å in Case-3 and -0.16 Å in Case-4, and the corresponding standard deviations σ are 0.035 Å, 0.041 Å, 0.044 Å and 0.045 Å. The above results demonstrate that the C-C bond stretch in Case-4 increases the inner radius (~0.08 Å) of the nanopore compared with Case-1, which may improve the possibility of C_3H_7Cl molecules crossing the nanopore. Compared with the atom A1, the deformation degree of B1 is slightly larger along the z direction as the membrane flexibility increases, but the basic deformation rules for them are similar (Figure S16). To understand the rearrangement of different carbon layers, we also captured the displacements of the carbon atoms A1~A4 and B1~B4 in the z direction in Case-4 (Figures 11 and S16). Obviously, the standard deviation σ of Δz of A1 is bigger than that of A4, revealing that the deformation degree of the carbon atoms at the pore edge is larger than the atoms away from the pore. It follows that the relaxation of the first carbon layer plays the more important role in pore geometry. The relaxation of 2~4 carbon layers may lead to micro-deformations of pores, which have little impact on the separation performance of the membrane. The simulation cases about H-pore-18 and H-pore-21 membranes with a higher flexibility are shown in Figures S17 and S18. As a result, we explored the three membranes H-pore-16, H-pore-18 and H-pore-21 to achieve the effective separation of C_3H_5Cl/C_3H_7Cl mixtures, even with high membrane flexibility.

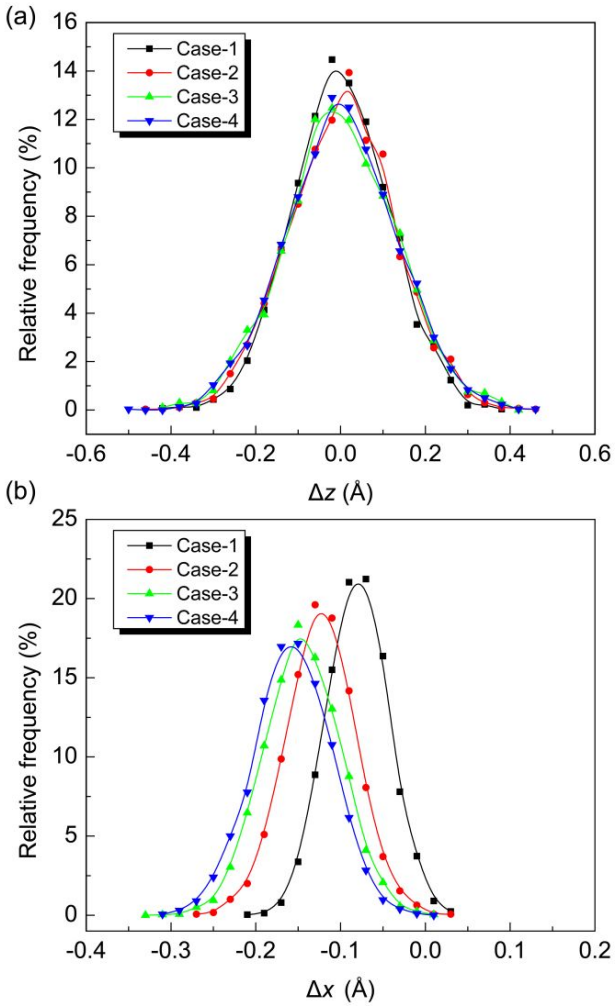

Figure 10. Frequency distributions for the displacements of the A1 carbon atom in the H-pore-16 membrane compared with the initial positions in different cases: (a) along the *z* direction and (b) along the *x* direction

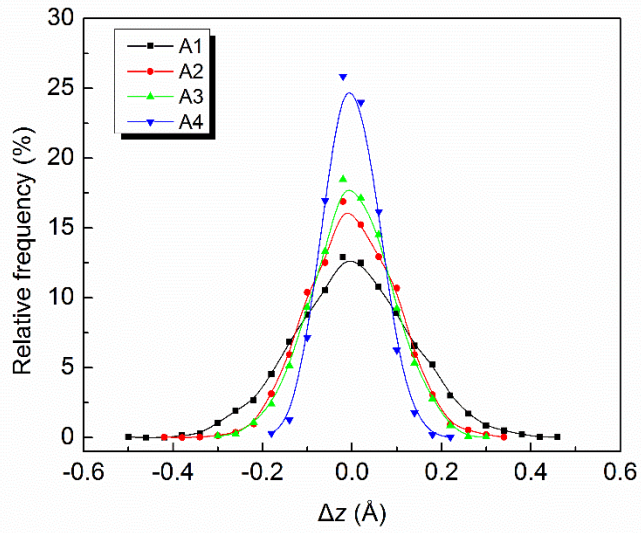

Figure 11. Frequency distributions for the displacements of the carbon atoms A1~A4 in the H-pore-16 membrane along the *z* direction when 4-layer carbon neighbours around the pore were relaxed in Case-4.

4. Conclusion

We have explored three NG membranes (H-pore-16, H-pore-18 and H-pore-21) with appropriate pore size and shape to effectively separate C_3H_5Cl/C_3H_7Cl mixtures with the ultrahigh selectivity. From molecular dynamics simulations, only C_3H_5Cl can pass through the three NG membranes with only H atoms and the first carbon layer around the pore relaxed. The deformation degree of the carbon atoms away from the pore is lower than that of the atoms at the pore edge, thereby exhibiting a little influence on the separation performance. Thermodynamically, C_3H_5Cl has a lower energy barrier of permeation than C_3H_7Cl and the NG membranes show preferential adsorption for C_3H_5Cl due to the vdW interaction, which reveal that the NG membranes prefer C_3H_5Cl molecules to cross the pores. According to the study on conformational energy, C_3H_5Cl has the lower energy penalty to twist to the cis-conformation that the pores prefer, thereby facilitating its penetration through the membranes. On the contrary, the case is different from C_3H_7Cl. Therefore, separating similar C_3H_5Cl/C_3H_7Cl mixtures with the ultrahigh selectivity could be achieved by constructing appropriate pore sizes and shapes which can restrict molecular conformation to pass through the pore. The conformation-induced mechanism outlined here may be able to purify other paraffin/olefin mixtures with the distinct difference of conformational energy barriers.

Conflicts of interest

There are no conflicts to declare.

Acknowledgment

This work was supported by Financial supports from the National Key R&D Program of China (2016YFB0301702), the National Natural Science Foundation of China (21490584, 91534105, 51808362, 21878298), Key Research Program of Frontier Sciences of CAS (QYZDJ-SSW-JSC030) and Key Research Program of Provincial Science and Technology Department in Sichuan (2017SZ0167).

References

1. A. Cadiau, K. Adil, P. M. Bhatt, Y. Belmabkhout and M. Eddaoudi, *Science*, 2016, **353**, 137-140.
2. L. Li, R. B. Lin, R. Krishna, X. Wang, B. Li, H. Wu, J. Li, W. Zhou and B. Chen, *Journal of the American Chemical Society*, 2017, **139**, 7733-7736.
3. P. Q. Liao, W. X. Zhang, J. P. Zhang and X. M. Chen, *Nature communications*, 2015, **6**, 8697.
4. H. Wang, X. Dong, V. Colombo, Q. Wang, Y. Liu, W. Liu, X. L. Wang, X. Y. Huang, D. M. Proserpio, A. Sironi, Y. Han and J. Li, *Advanced materials*, 2018, 1805088.
5. K. J. Chen, D. G. Madden, T. Pham, K. A. Forrest, A. Kumar, Q. Y. Yang, W. Xue, B. Space, J. J. t. Perry, J. P. Zhang, X. M. Chen and M. J. Zaworotko, *Angewandte Chemie*, 2016, **55**, 10268-10272.
6. E. L. First, C. E. Gounaris and C. A. Floudas, *Langmuir,* 2013, **29**, 5599-5608.
7. C. Gucuyener, J. van den Bergh, J. Gascon and F. Kapteijn, *Journal of the American Chemical Society*, 2010, **132**, 17704-17706.
8. S. Rafiq, Z. Man, A. Maulud, N. Muhammad and S. Maitra, *Separation and Purification Technology*, 2012, **90**, 162-172.
9. J. Zhang, N. Burke, S. Zhang, K. Liu and M. Pervukhina, *Chemical Engineering Science*, 2014, **113**, 54-61.
10. Z. Kang, M. Xue, L. Fan, L. Huang, L. Guo, G. Wei, B. Chen and S. Qiu, *Energy & Environmental Science*, 2014, **7**, 4053-4060.
11. G. P. Lithoxoos, A. Labropoulos, L. D. Peristeras, N. Kanellopoulos, J. Samios and I. G. Economou, *The Journal of Supercritical Fluids*, 2010, **55**, 510-523.

12. L. Meng, X. Zou, S. Guo, H. Ma, Y. Zhao and G. Zhu, *ACS Appl Mater Interfaces*, 2015, **7**, 15561-15569.

13. H. Li, Z. Song, X. Zhang, Y. Huang, S. Li, Y. Mao, H. J. Ploehn, Y. Bao and M. Yu, *Science*, 2013, **342**, 95-98.

14. F. Macedonio and E. Drioli, *Engineering*, 2017, **3**, 290-298.

15. B. Raghavan and T. Gupta, *Journal of Physical Chemistry C*, 2017, **121**, 1904-1909.

16. S. C. O'Hern, M. S. Boutilier, J. C. Idrobo, Y. Song, J. Kong, T. Laoui, M. Atieh and R. Karnik, *Nano letters*, 2014, **14**, 1234-1241.

17. D. V. Verschueren, W. Yang and C. Dekker, *Nanotechnology*, 2018, **29**, 145302.

18. M. D. Fischbein and M. Drndić, *Applied Physics Letters*, 2008, **93**, 113107.

19. S. P. Surwade, S. N. Smirnov, I. V. Vlassiouk, R. R. Unocic, G. M. Veith, S. Dai and S. M. Mahurin, *Nature Nanotechnology*, 2016, **11**, 995-995.

20. H. Liu, Z. Chen, S. Dai and D.-e. Jiang, *Journal of Solid State Chemistry*, 2015, **224**, 2-6.

21. L. W. Drahushuk and M. S. Strano, *Langmuir*, 2012, **28**, 16671-16678.

22. K. Solvik, J. A. Weaver, A. M. Brockway and J. Schrier, *Journal of Physical Chemistry C*, 2013, **117**, 17050-17057.

23. H. Liu, S. Dai and D. E. Jiang, *Nanoscale*, 2013, **5**, 9984-9987.

24. Y. Wang, Q. Yang, C. Zhong and J. Li, *Applied Surface Science*, 2017, **407**, 532-539.

25. G. Liu, W. Jin and N. Xu, *Chemical Society Reviews*, 2015, **44**, 5016-5030.

26. B. Yuan, H. Sun, T. Wang, Y. Xu, P. Li, Y. Kong and Q. J. Niu, *Scientific Reports*, 2016, **6**, 28509.

27. X. Wang, R. Krishna, L. Li, B. Wang, T. He, Y.-Z. Zhang, J.-R. Li and J. Li, *Chemical Engineering Journal*, 2018, **346**, 489-496.

28. S. Lifson, A. T. Hagler and P. Dauber, *Journal of the American Chemical Society*, 1979, **101**, 5111-5121.

29. S. Plimpton, *Journal of Computational Physics*, 1995, **117**, 1-19.

30. Y. Wang, Q. Yang, J. Li, J. Yang and C. Zhong, *Physical Chemistry Chemical Physics*, 2016, **18**, 8352-8358.

31. M. Shan, Q. Xue, N. Jing, C. Ling, T. Zhang, Z. Yan and J. Zheng, *Nanoscale*, 2012, **4**, 5477-5482.

32. L. Wang, M. S. H. Boutilier, P. R. Kidambi, D. Jang, N. G. Hadjiconstantinou and R. Karnik, *Nature Nanotechnology*, 2017, **12**, 509-522.
33. C. J. Russo and J. A. Golovchenko, *Proceedings of the National Academy of Sciences of the United States of America*, 2012, **109**, 5953-5957.
34. D. J. Murray, D. D. Patterson, P. Payamyar, R. Bhola, W. Song, M. Lackinger, A. D. Schluter and B. T. King, *Journal of the American Chemical Society*, 2015, **137**, 3450-3453.
35. J. P. Perdew, K. Burke and M. Ernzerhof, *Physical Review Letters*, 1996, **77**, 3865-3868.
36. B. Delley, *Journal of Chemical Physics*, 1990, **92**, 508-517.
37. A. Tkatchenko and M. Scheffler, *Physical Review Letters*, 2009, **102**.
38. K. Nieszporek and M. Drach, *Physical Chemistry Chemical Physics*, 2015, **17**, 1018-1024.
39. T. Wu, Q. Xue, C. Ling, M. Shan, Z. Liu, Y. Tao and X. Li, *Journal of Physical Chemistry C*, 2014, **118**, 7369-7376.
40. Z. Yuan, A. Govind Rajan, R. P. Misra, L. W. Drahushuk, K. V. Agrawal, M. S. Strano and D. Blankschtein, *ACS nano*, 2017, **11**, 7974-7987.
41. A. W. Hauser and P. Schwerdtfeger, *Physical Chemistry Chemical Physics,* 2012, **14**, 13292-13298.

Conformation-induced separation that C_3H_5 twisting to the pore preferred cis-conformation with lower energy penalty than C_3H_7 can cross the nanopore.